G. Catalysis by First Principles

C. K. Narula, L. F. Allard, V. Bhirud, B. Gates, M. Moses, W. Schneider, W. Shelton, Y. Xu
Oak Ridge National Laboratory
P.O. Box 2008, MS 6116
Oak Ridge, TN 37831-6116
(865) 574-8445, fax: (865) 576-6298; e-mail: narulack@ornl.govl

DOE Technology Development Area Specialist: James J. Eberhardt
(202) 586-9837; fax: (202) 586-1600; e-mail: james.eberhardt@ee.doe.gov
ORNL Technical Advisor: D. Ray Johnson
(865) 576-6832; fax: (865) 574-6098; e-mail: johnsondr@ornl.gov

---

Contractor: Oak Ridge National Laboratory, Oak Ridge, Tennessee
Prime Contract No: DE-AC05-00OR22725

Objective

Search for durable emission catalysts [lean No_x (nitrogen oxides) trap (LNT), three-way catalyst (TWC), OC] from a protocol based on

- an integrated approach between computational modeling and experimental development
- design and testing of new catalyst materials to rapidly identify the key physiochemical parameters necessary for improving the catalytic efficiency of these materials.

Approach

- Theoretical modeling
  - Density functional theory-based first-principles calculations
  - Optimization of platinum (Pt) clusters supported on alumina
  - Interaction of CO, NO_x, and hydrocarbons (HCs) with Pt clusters supported on alumina
- Experimental system
  - Synthesize Pt and rhenium (Re) nanoclusters on morphologically diverse alumina supports
  - Evaluate systems for CO, NO_x, and HC oxidation

Accomplishments

- Completed the synthesis of a series of Pt and Re clusters supported on commercial alumina.
  - The microstructural studies of freshly prepared Pt/alumina (by impregnation) show it to contain 10–20 atom clusters. Thermal treatment leads to larger particles.
  - The microstructural studies of freshly prepared Re/alumina (by impregnation) show it to contain 10–20 atom clusters. We prepared smaller clusters of 1–3 atoms from the decarbonylation of $H_3Re_3(CO)_{12}/\gamma–Al_2O_3$. Thermal treatment leads to larger particles.
- Synthesized alumina sol-gel and molecular sieve support materials and began efforts to increase the thermal stability of the molecular sieves.
- Carried out modeling of isolated Pt clusters. Theory tells us that the following are true for Pt nanoclusters:
  - Reactivity (adsorption) shows strong size dependence.

- — Smaller clusters are much more prone to oxidation.
- — Oxidized clusters adopt 1-dimensional or 2-dimensional structures.
- — In an O_2 atmosphere, higher T or lower p_{O2} leads to lower extent of oxidation and makes the reduction of oxidized Pt clusters more facile → Pt oxides becoming better oxidizing agent.
- — Lower oxide phases are more prevalent for larger clusters.

- Equipped the synthesis laboratory to enable preparation of catalyst materials under inert conditions. A benchtop catalyst testing reactor has been installed (funded by a project from DOE Office of Industrial Technologies) and is being tested before catalyst evaluation experiments start.

Future Direction

- Understand the structures of nanoclusters on support. Our results show that nano-clusters are 10–15 atoms.
  - — Develop theoretical models to understand cluster oxidation state (oxidized, reduced, in equilibrium), dependence on cluster size, and the kinetics of oxidation.
  - — Conduct experimental studies on the structures of these systems using X-ray absorption fine structure (EXAFS) and X-ray absorption near-edge structure (XANES).
- Support interaction with clusters and its impact on the structure and reactivity:
  - — cationic or zero-valent metals or both
  - — cationic metals at the metal–support interface
- Analyze the reactivity of the clusters
  - — Conduct theoretical and experimental studies on structure-reactivity correlation toward CO, NO_x, and HC oxidation studies
  - — Determine the impact of cluster size on catalytic activity
- Translate these results into the design of durable supported catalysts for LNTs (and other systems such as TWC, OC for diesel)

Introduction

This research focuses on an integrated approach between computational modeling and experimental development, design, and testing of new catalyst materials, which we believe will rapidly identify the key physiochemical parameters necessary for improving the catalytic efficiency of these materials.

The typical solid catalyst consists of nanoparticles on porous supports. The development of new catalytic materials is still dominated by trial-and-error methods, even though the experimental and theoretical bases for their characterization have improved dramatically in recent years. Although it has been successful, the empirical development of catalytic materials is time-consuming and expensive and brings no guarantee of success. Part of the difficulty is that most catalytic materials are highly non-uniform and complex, and most characterization methods provide only average structural data. Now, with improved capabilities for synthesis of nearly uniform catalysts—which offer the prospects of high selectivity as well as susceptibility to incisive characterization combined with state-of-the science characterization methods, including those that allow imaging of individual catalytic sites—we have a compelling opportunity to markedly accelerate the advancement of the science and technology of catalysis.

Computational approaches, on the other hand, have been limited to examining processes and phenomena using models that had been much simplified compared with real materials. This limitation was mainly a consequence of limitations in computer hardware and in the development of sophisticated algorithms that are computationally efficient. In particular, experimental catalysis has not benefited from the recent advances in high-performance computing that enable more realistic simulations (empirical and first-principles) of large ensemble atoms, including the local environment of a catalyst site in heterogeneous catalysis. These types of

simulations, when combined with incisive microscopic and spectroscopic characterization of catalysts, can lead to a much deeper understanding of the reaction chemistry that is difficult to decipher from experimental work alone.

Thus a protocol to systematically find the optimum catalyst can be developed that combines the power of theory and experiment for atomistic design of catalytically active sites and can translate the fundamental insights gained directly to a complete catalyst system that can be technically deployed (Figure 1).

Although it is no doubt computationally challenging, the study of surface, nanometer-sized, metal clusters may be accomplished by merging state-of-the-art, density-functional-based electronic-structure techniques and molecular-dynamic techniques. These techniques provide accurate energetics, force, and electronic information. Theoretical work must be based on electronic-structure methods, as opposed to more empirical-based techniques, so as to provide realistic energetics and direct electronic information.

A computationally complex system, in principle, will be a model of a simple catalyst that can be synthesized and evaluated in the laboratory. It is important to point out that such a system for an experimentalist will be an idealized simple model catalyst system that will probably model a "real-world" catalyst.

Thus it is conceivable that a "computationally complex but experimentally simple" system can be examined by both theoretical models and experimental work to forecast improvements to obtain optimum catalyst systems.

Approach

The theoretical modeling is based on density-functional theory (DFT) studies of Pt clusters to understand the relationship between cluster size, structure, composition, and reactivity. This, coupled with first-principles thermodynamics, provides insights into the effects of oxidizing atmosphere (O_2)—finite (T, p_{O2}), structure, composition, and redox potential on particle size. The results provide guidance for investigations of larger/supported clusters. The next steps of this work will model supported clusters, based on input from experimental results, and their interactions with CO, NO_x, and HC.

Experimentally, we have synthesized a series of Pt and Re clusters and particles supported on morphologically different γ–aluminas. The microstructural characterization reveals structural differences in 1–3 atom and 10–20 atom clusters. We will evaluate these catalysts for their CO, NO_x, and HC oxidation capability. Guided by the theoretical models and experimental results, we will synthesize a new set of catalyst materials with higher durability under operating conditions.

Results

Over the last year, theoretical studies have been carried out on the oxidation behavior of gas-phase Pt nanoparticles and metallic clusters. On the experimental side, a range of γ–Al_2O_3 supported Pt and Re clusters have been synthesized and characterized. Alumina sol-gels and molecular sieves have also been synthesized to use as supports. The results are summarized in the following subsections.

Alumina Support Materials

We synthesized sol-gel alumina by the reported procedure from the hydrolysis of $Al(sec\text{-}C_4H_9O)_3$, nitric acid peptization, and gelation. The material gives an amorphous X-ray diffraction between 5 and 70° 2θ. The alumina sol surface area calculated from a multipoint BET (Brunauer, Emmett, and Teller) measurement without degassing is 170.82 m^2/g. Scanning electron microscopy (SEM) images show some macro-pores on the surface, but no ordered structure can be seen (Figure 2).

For the synthesis of alumina molecular sieves, we employed a structure-templated method using

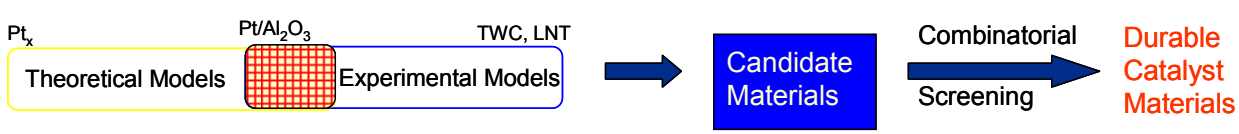

Figure 1. Theory and experiment, combined with simulation, can translate to a deployable catalyst system.

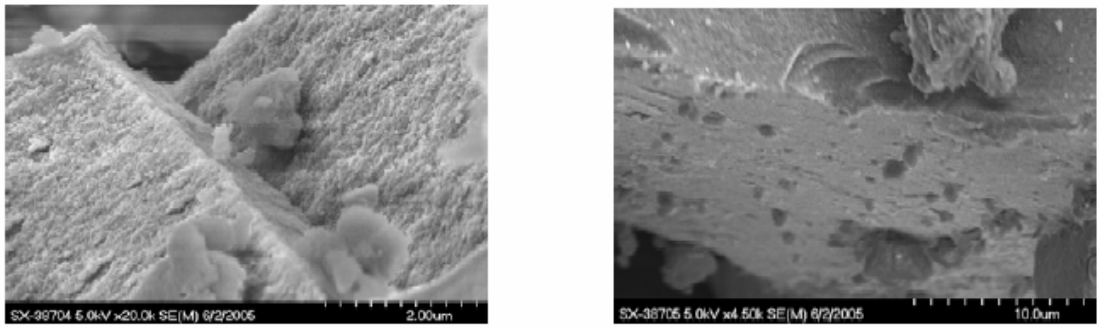

Figure 2. SEM images of sol-gel alumina.

cetyltrimethylammonium bromide, reported by Deng et al.[1] X-ray diffraction (XRD) of the alumina molecular sieves and SEM images (Figure 3) confirm the reproducibility of this synthetic route. Since the rate of stirring has a significant impact on the morphological structure of alumina molecular sieves, we carried out the synthesis using a magnetic stirrer and used stirring rates of 64 and 128 rpm. The BET surface areas of 128-rpm and 64-rpm samples were 208 m^2/g and 234 m^2/g, respectively. These values are about half of the reported BET surface areas (~470 m^2/g). Efforts are in progress to determine an accurate BET surface area before undertaking further modifications to the synthesis procedure.

Since the alumina molecular sieve structure collapses at elevated temperatures, we are exploring synthetic routes to incorporate stabilizers into the alumina molecular sieve structure. Employing the Pinnavaia method, we added lanthanum (La)

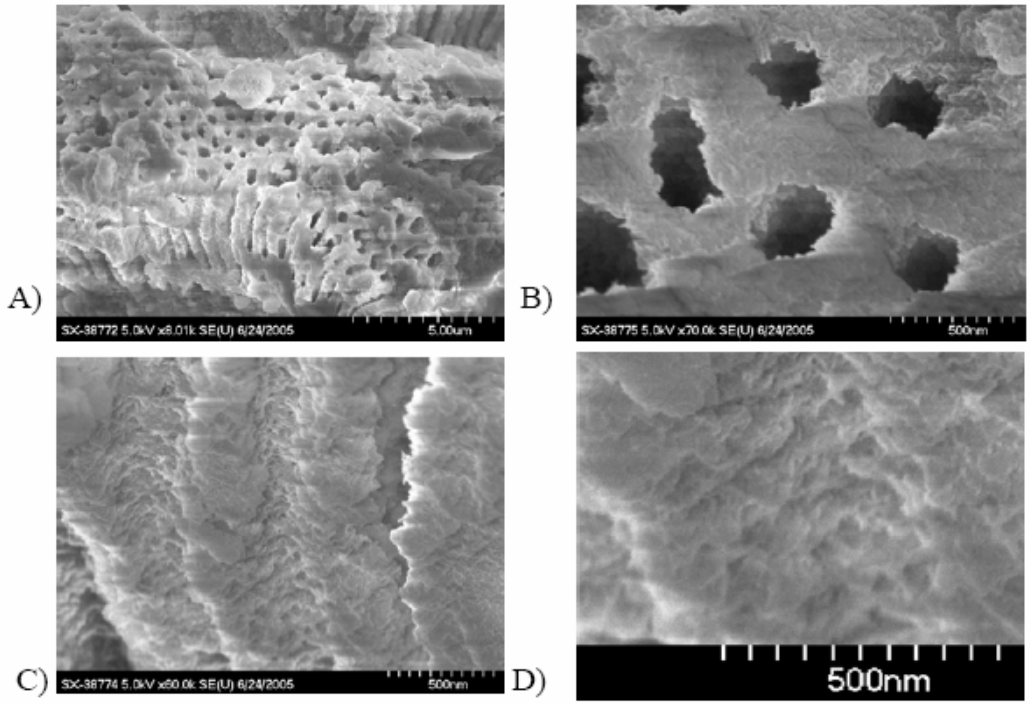

Figure 3. SEM images of the Al_2O_3 molecular sieves prepared by stirring at 64 rpm (a) shows the surface openings of the macropores (channel openings) and the channels that extend through the material. (b) is a close-up of the channel opening at an angle. (c) is close-up of macropore channels and some of the micropores within the channels can be discerned (d) shows an enlargement of the micropores within the channels from (c).

nitrate during the synthesis of alumina molecular sieves. This method did not lead to improved thermal durability of alumina molecular sieves. The powder XRD (Figure 4) of 2 wt % La-doped alumina molecular sieves, after calcining at 500°C/ 5.5 h in flowing air, exhibits no diffraction peaks, suggesting that the materials are amorphous materials. Further calcining at 700°C/5.5h and 900°C/5.5 h led to low-intensity broad peaks in powder XRD that were assigned to aluminum oxide. The SEM of La-impregnated samples resembled that of pure alumina molecular sieves after initial calcining at 500°C/5.5h (Figure 5). The impact of calcining La-impregnated alumina molecular sieves for 5.5 h at 700°C after the initial 500°C/ 5.5 h can be seen in the SEM (Figure 6). The structures

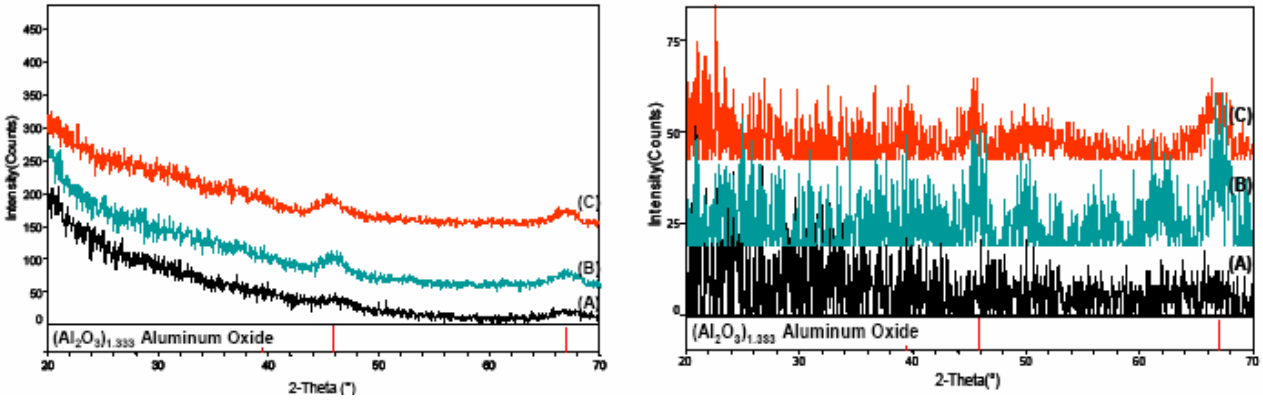

Figure 4. X-ray diffraction patterns of Al_2O_3 molecular sieves synthesized at 64 rpm, doped with 2 wt % La and calcined under flowing air at (a) 500°C/5.5 h, followed by annealing at (b) 700°C/5.5 h, and finished with a final annealing at (c) 900°C/5.5 h. The diffraction patterns on the left are without background subtraction and those on the right are with background subtraction. Diffraction lines of aluminum oxide are of JCPDF # 75-0921.

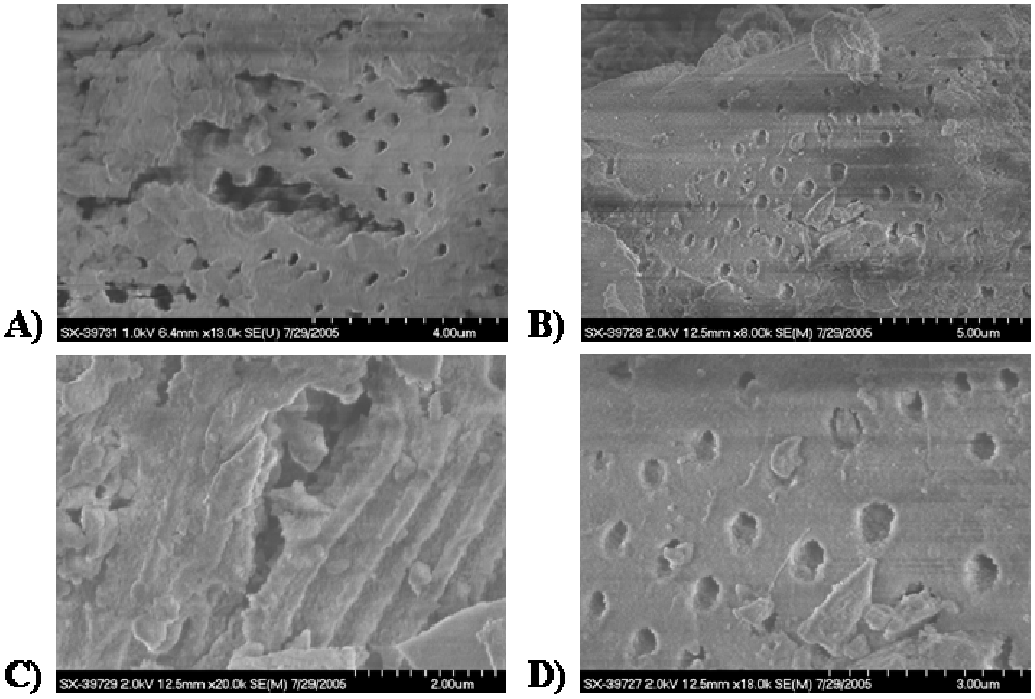

Figure 5. SEM images of the Al_2O_3 molecular sieves impregnated with 2% La and calcined at 500°C/5.5h. The images show the surface openings of the macropores (channel openings) and the channels that extend through the material.

of many porous channels were maintained; however, the coverage and uniformity of the channels have diminished. This suggests that La did not get incorporated in the molecular sieve structure. As a next step, we will explore our method of employing heterometallic alkoxides as precursors for the incorporation of La in alumina molecular sieves.

Platinum-Alumina System

While synthesis and characterization of sol-gel and molecular sieve alumina are in progress, we have synthesized and characterized Pt/Al_2O_3 materials using commercial alumina. We carried out the synthesis of nanocluster Pt/commercial γ–alumina by impregnation of γ–alumina with $H_2PtCl_6 \cdot 6H_2O$ followed by calcination in air. The scanning transmission electron microscopy (STEM) of 2% $Pt/\gamma–Al_2O_3$ (Figure 7) shows approximately 1-nm particles with a narrow distribution centered in the 1–1.5-nm range (Figure 7B). High-magnification images obtained using the aberration-corrected electron microscope (ACEM) in the HAADF-STEM mode indicate particles of 10–20 atoms and also show some smaller platinum clusters (Figure 7c and d).

Thermal treatment of this material leads to ~10-nm or larger Pt clusters supported on γ–alumina with the Pt particle size depending on the temperature and duration of thermal treatment. In order to prepare smaller clusters, a possible approach is to synthesize platinum carbonyl clusters on alumina. A variety of Pt carbonyl clusters $\{[Pt_{15}(CO)_{30}]^{2-}$, $[Pt_6(CO)_{12}]^{2-}$, $[Pt_9(CO)_{18}]^{2-}\}$ on MgO are known.[2] A synthesis of such clusters on a variety of aluminas (commercial γ–alumina, sol-gel alumina[2] and molecular sieve alumina[1] will be challenging, but a simple decarbonylation will furnish Pt clusters of fewer than 10 atoms.

The theoretical efforts, which are based on DFT, have so far been focused on the effect of cluster size and the impact of oxidation on the properties—including structure, composition, and

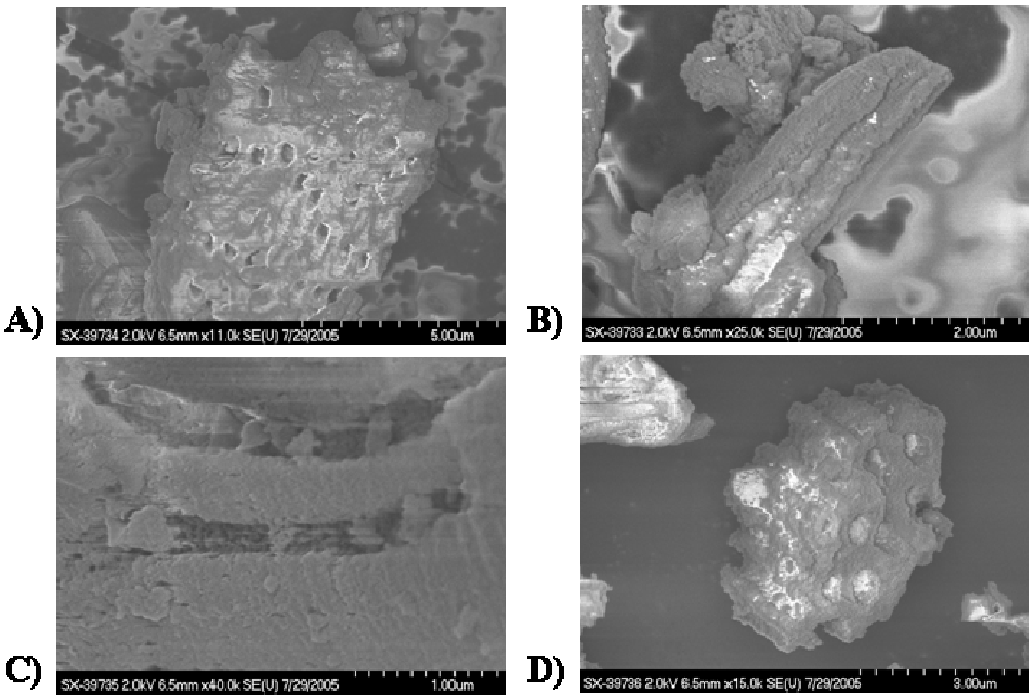

Figure 6. SEM images of the Al_2O_3 molecular sieves impregnated with 2% La and calcined first at 500°C/5.5h followed by further calcination at 700°C/5.5h (a) shows the surface openings of the macropores (channel openings) (b) shows a piece of alumina with channels that extend through the material (c) shows some channels that do not appear to extend through the entire piece of alumina (d) show a piece of alumina with a honeycomb structure.

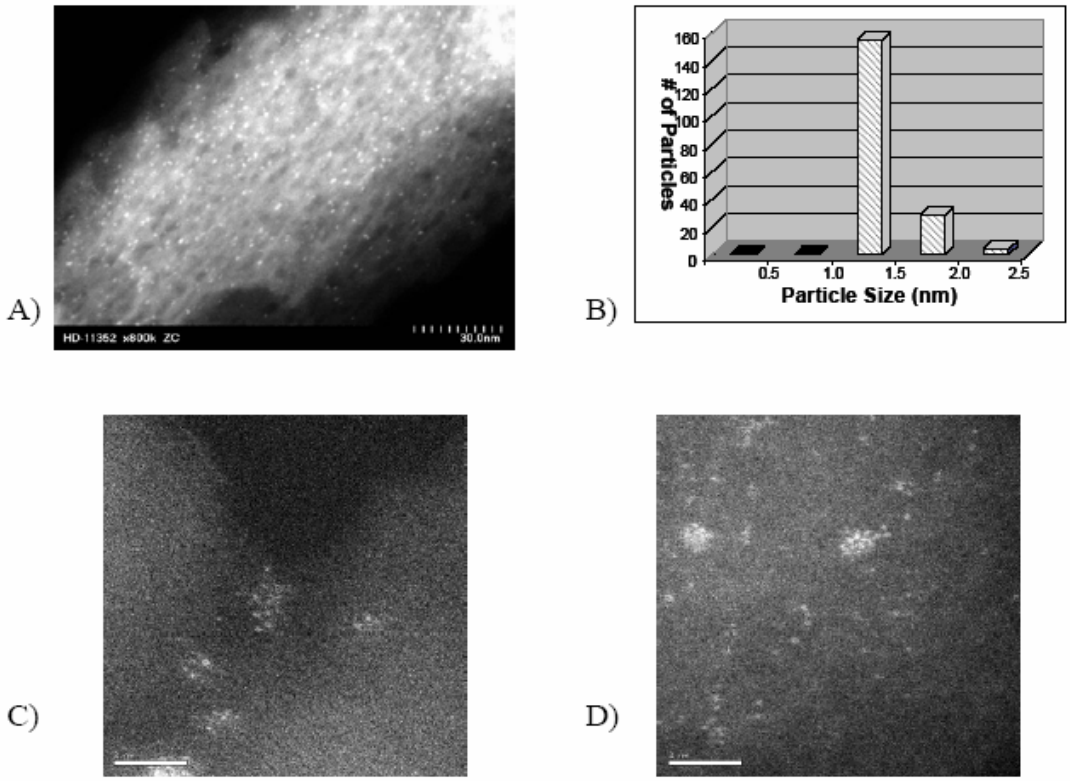

Figure 7. (a) STEM images of the 2% Pt/γ-Al_2O_3 sample and (b) the particles size distribution. (c and d) ACEM HAADF-STEM images of 2% Pt/γ-Al_2O_3.

reactivity—of isolated Pt clusters. We have concluded the investigation of Pt_x nanoclusters (x = 1, 2, 3, 4, 5, and 10) using the DFT codes VASP and Dacapo. The main results are summarized in Figure 6.

A salient feature is that the oxidation of the Pt clusters, either partial or complete, is more exothermic (more negative oxidation energy) than the oxidation of bulk Pt to the bulk oxides. The oxidation energies display strongly non-linear dependence on cluster size and generally become more exothermic as the size decreases. This means that smaller Pt clusters are much more prone to oxidation than larger Pt clusters or bulk Pt. Complete oxidation of a Pt_x cluster to Pt_xO_{2x} is favored energetically over partial oxidation to Pt_xO_x, regardless of the cluster size.

Upon oxidation, the structure of Pt clusters also changes substantially. Whereas the original Pt clusters are generally 3-dimensional, the oxidized clusters prefer flatter, 1- or 2-dimensional shapes. The Pt_xO_x clusters form closed loops, in which the Pt atoms adopt the shapes of triangles, quadrangles, pentagons, etc., with each Pt atom coordinated to two O atoms. The Pt_xO_{2x} series, on the other hand, form open, bent linear chains, in which the middle Pt atoms are each coordinated to four O atoms. The structure of the oxidized Pt clusters is also very different from the 3-dimensional matrices of the bulk oxides (Figure 8).

Bader charge analysis of the oxidized Pt nanoclusters reveals another difference between the oxidized Pt nanoclusters and the corresponding bulk oxides: the Pt-O bonds in the clusters have considerably less ionic character than those in the bulk oxides.

Both cluster size and oxidation affect the reactivity of the Pt clusters. We studied the adsorption energies of O, O_2, CO, and CO_2 on the $Pt_{1–5}$ clusters and found considerable variation with respect to cluster size. In general, adsorption on smaller clusters is more exothermic. The adsorption energies of O, O_2, and CO_2 exhibit a minimum of around x = 4 before approaching the level on an extended Pt

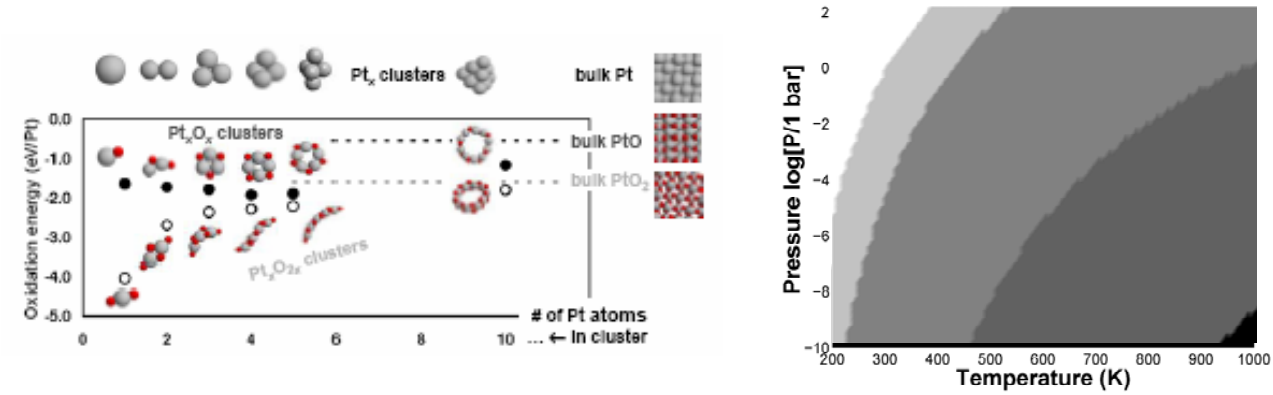

Figure 8. (Left) Oxidation energies of the Pt_xO_x (filled circles) and Pt_xO_{2x} (open circles) clusters. Black and grey dashed lines indicate bulk PtO (–0.54 eV) and β-PtO2 (–1.58 eV) formation energies, respectively. The stick-and-ball representations of the pure Pt and Pt oxide clusters are included. Red spheres represent O atoms, and grey spheres represent Pt atoms. The stoichiometries of Pt:O = 1:1 and 1:2 represent, respectively, partially and fully oxidized Pt systems. (Right) A temperature-O_2 pressure phase diagram of Pt clusters from first-principles thermodynamic model.

surface. CO adsorption grows monotonically weaker with increasing cluster size. The adsorption energies of O and CO are found to be weaker on several Pt_xO_x clusters than on the corresponding pure Pt_x clusters, suggesting that oxidation probably weakens the adsorption of atoms and molecules in general.

Since DFT results are formally obtained at 0 K and in vacuum, we developed a first-principles thermodynamic model in order to incorporate the effects of an oxygen atmosphere with finite temperature and pressure on the composition of the Pt clusters (Figure 8). A temperature–O_2 pressure phase diagram has been constructed for each of the Pt_{1-3} clusters. The results agree with the general physical insight that higher temperature or lower pressure favors lower extent of oxidation. Under conditions of interest to this project—e.g., diesel engine exhaust, which is generally found in the 400–600 K range and has an O_2 partial pressure of ~0.1 bar—the extent of oxidation is found to decrease from a dioxide to a monoxide stoichiometry with increasing cluster size. No sub-monoxides are seen in any of the three phase diagrams. Therefore, we expect larger clusters to exist primarily as monoxides under similar conditions.

In summarizing the theoretical findings, we note that both size and oxidation profoundly affect the structure, composition, and reactivity of Pt clusters, at least in the size range that we have studied so far. In the second year of this project, we will tackle the effect of another variable on the properties of Pt clusters, namely the metal oxide support that is an integral part of many heterogeneous catalysts, including automotive applications (e.g., TWC and LNT). We will study the reactivity of larger clusters, perhaps with sizes in the range of 10–20 Pt atoms, which are more accessible to current laboratory techniques. Our results so far have provided many hints that will facilitate the modeling of larger clusters and the investigation of support effects.

Theoretical study also suggests that the structure of experimentally observed 10–20 atom Pt-clusters is different from that of bulk metal and in all likelihood has some oxygen incorporated. Three-dimensional structure mapping and EXAFS studies are in progress to determine detailed cluster structure.

Rhenium-Alumina System

Since Pt-carbonyl cluster chemistry on alumina is not well developed, we chose Re-carbonyl clusters supported on alumina as surrogates for Pt-alumina clusters of fewer than 10 atoms. We initiated this work by successfully synthesizing $H_3Re_3(CO)_{12}$ by using literature methods and confirmed its formation by infrared spectroscopy.[4] In the previous report, we described the decarbonylation and characterization of decarbonylated clusters by EXAFS and XANES spectroscopy. The EXAFS parameters indicated complete decarbonylation of the Re. The data indicate the formation of tri-nuclear Re rafts, Re_3. The decarbonylated samples, modeled as tri-rhenium

rafts, are shown by the XANES data to incorporate electron-deficient (cationic) Re. On the basis of a comparison of the observed XANES signature with various XANES of various reference materials, we tentatively identify the oxidation state of Re to be +4. This statement is rough and in need of theoretical assessment.

The $H_3Re_3(CO)_{12}/\gamma–Al_2O_3$ sample was imaged on the ACEM in the HAADF-STEM mode. The intact supported tri-rhenium rafts indicated by infrared spectra, EXAFS, and XANES were confirmed by atomic-resolution STEM images (Figure 9 and inset). In addition to tri-rhenium rafts, atomic rhenium, dimers, and larger polyatomic clusters were also atomically resolved. STEM images indicate that although slightly larger clusters were present, the sample was predominately clusters comprising 1–3 Re atoms.

STEM images of $H_3Re_3(CO)_{12}/\gamma–Al_2O_3$ treated in H_2 at 400°C to decarbonylate the clusters were also obtained using the ACEM. Images at high magnification indicated uniform clusters with diameters of approximately 0.4–0.8 nm. The instability of the microscope at the time of use hindered efforts to capture images of atomic resolution. Rhenium has a radius of 1.37 Å, which suggests that the clusters are composed of 1–3 Re atoms.

Decarbonylation of $H_3Re_3(CO)_{12}/\gamma–Al_2O_3$ was also done by treatment in helium at 400°C. STEM images show metallic particles in the 1.4–3.9 nm range (Figures 10 and 11). Some small Re clusters were also present, but because of the 3-dimensional structure of the metallic nanoparticles, imaging was difficult.

Interestingly, $Re/\gamma–Al_2O_3$ synthesized by $ReCl_5$ impregnation on commercial $\gamma–Al_2O_3$ and subsequt calcining led to small (1–1.5 nm) clusters. Microstructural characterization on the ACEM shows two types of areas. In one type of area (Figure 12), 10–20-atom clusters of essentially 1 nm were observed that were reminiscent of our $Pt/\gamma–Al_2O_3$ materials (Figure 8). While these clusters are not completely random in the atomic arrangement, a 3-dimensional metallic order is not observed. The second area (Figure 13) shows smaller, less uniform clusters and single-atom structures. Neither area shows significant structure change as a result of time under the beam, suggesting a stabilizing interaction between Re and the support. The inconsistent loading may be attributed to the high Re loading.

Conclusions

We have prepared and characterized Pt and Re clusters of different sizes and properties (metallic and non-metallic) on commercial $\gamma–Al_2O_3$ ranging from single atoms to 2-nm 3-dimensional nanoparticles. Two other alumina supports with different structural properties, sol-gel and molecular sieves,

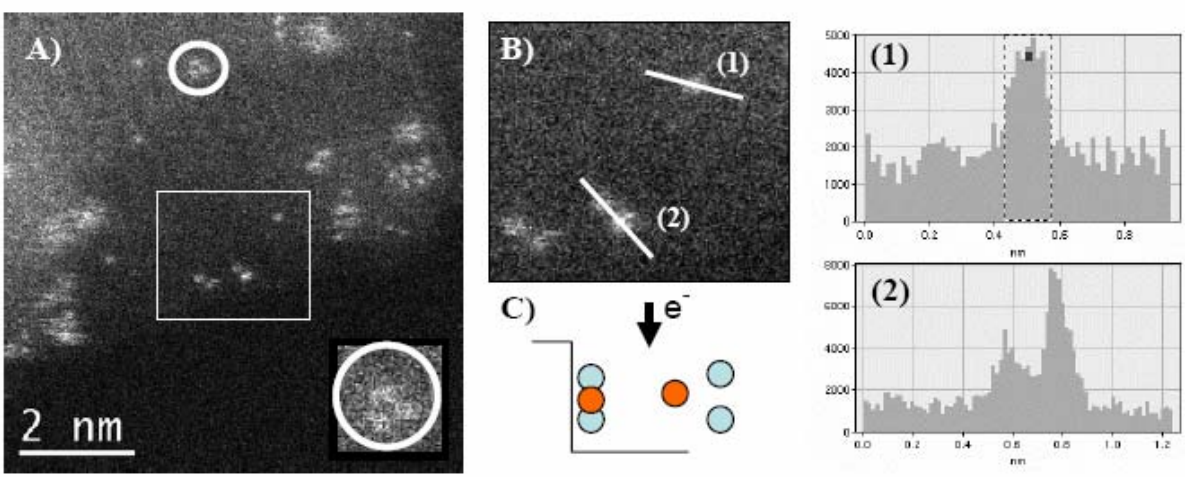

Figure 9. ACEM HAADF-STEM images of 1 wt % $Re/\gamma\text{-}Al_2O_3$. (a) Image of $H_3Re_3(CO)_{12}/\gamma\text{-}Al_2O_3$; the inset at the bottom right is an enlargement of the tri-rhenium raft located in the circle. (b) An enlargement of the boxed in area of (a). Traces 1 and 2 correspond to the particle intensity. Graphs indicate one atom in trace of particle (1) and three atoms in trace of particle (2). (c) Front and side views of Re3 cluster, tethered to a ledge parallel to the beam direction.

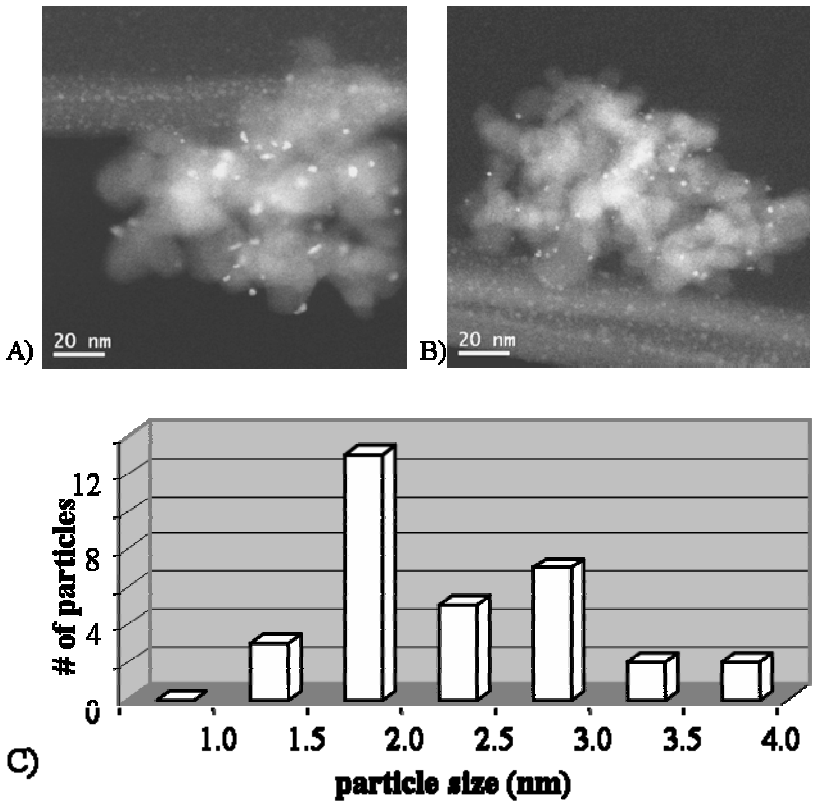

Figure 10. (a–b) show aberration corrected STEM-HAADF images of two different Re/γ-Al_2O_3 particles prepared by decarbonylating $[H_3Re_3(CO)_{12}]$/γ-Al_2O_3 in He at 400°C, and (c) shows the Re particle size distribution.

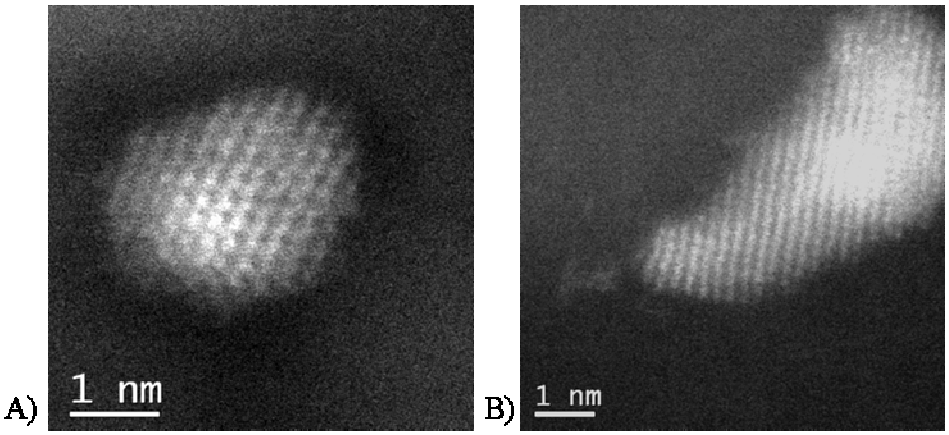

Figure 11. The high magnification ACEM images show the 3D metallic structure of the Re particles prepared by decarbonylating $[H_3Re_3(CO)_{12}]$/γ-Al_2O_3 in He at 400°C.

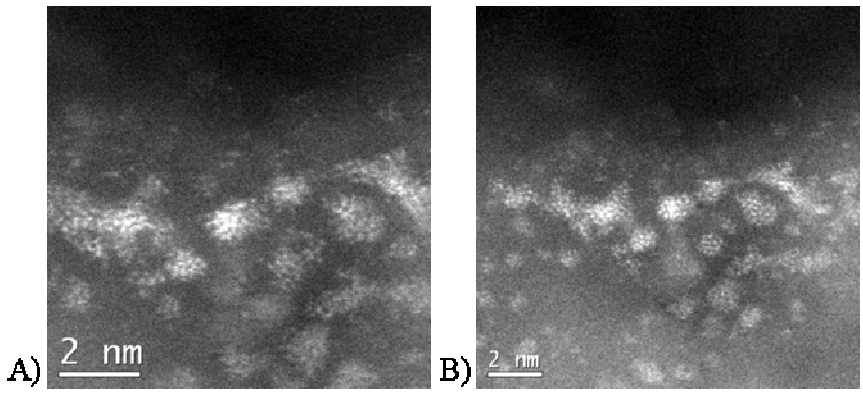

Figure 12. These ACEM images Re/γ-Al_2O_3 prepared by impregnation. The images were taken consecutively showing no movement of the clusters.

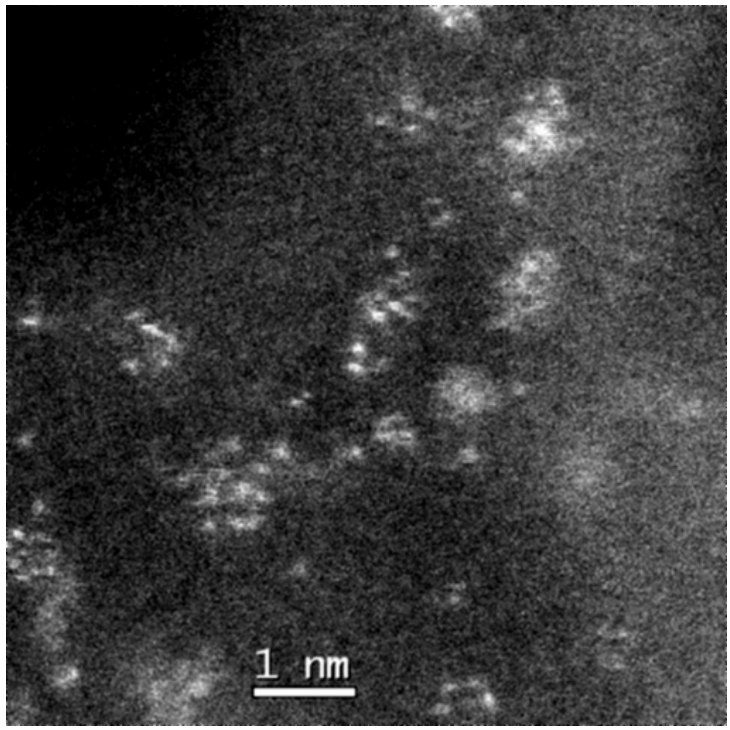

Figure 13. This high magnification ACEM image shows Re atoms and small clusters of Re/γ-Al_2O_3 prepared by impregnation method.

are being prepared and will soon be ready for Pt and Re loading. Computational calculations and simulation have shown the oxidation behavior of small Pt clusters and their energetically favored structures.

Our next goals are to finish structural characterization and preparation of the clusters supported on the three different alumina supports, obtain and compare their activity as CO oxidation catalysts, and use the experimental data as the inputs for the theoretical models.

Presentations and Publications

C. K. Narula, presentation at the Eighth DOE Crosscut Workshop on Lean Emissions Reduction Simulation, Dearborn, Michigan, May 17–19, 2005.

L. F. Allard, presentation at the annual meeting of the Microscopy Society of America.

C. K. Narula, presentation at DEER 2005, Chicago, August 21–25, 2005.

Bruce Gates and W. Schneider, presentations at the North American Catalysis Society meeting, Philadelphia, May 22–27, 2005.

V. A. Bhirud, C. Narula, and B. C. Gates, "γ-Al_2O_3 Supported Tri-rhenium Rafts: Spectroscopic and Microscopic Characterization," in *Proceedings of the 19th North American Catalysis Society Meeting*, Philadelphia, May 22–27, 2005.

Y. Xu, W. A. Shelton, and W. F. Schneider, "Effect of Particle Size on the Oxidizability of Platinum Clusters," submitted to *J. Phys. Chem. A*.

Y. Xu, W. A. Shelton, and W. F. Schneider, "Nanoscale Effects in the Reactivity of Pt Clusters towards CO oxidation," in *Proceedings of the 19th North American Catalysis Society Meeting*, Philadelphia, May 22–27, 2005.

Y. Xu, W. A. Shelton, and W. F. Schneider, "Theoretical Studies Based on Post-Hartree-Fock and DFT Methods," in *Synthesis and Applications of Oxide Nanoparticles and Nanostructures*, ed. J. A. Rodriguez, John Wiley and Sons; in preparation.

V. A. Bhirud, M. J. Moses, D. A. Blom, L. F. Allard, Jr., T. Aoki, S. Mishina, C. K. Narula, and B. C. Gates, "Alumina-supported Tri-rhenium Clusters Visible by Aberration-Corrected Dark-field STEM," *Microscopy and Microanalysis 2005*, Honolulu, July 31–August 4, 2005.

C. K. Narula, W. A. Shelton, L. F. Allard, Y. Xu, M. Moses, W. Schneider, and B. Gates, "Combining Theory and Experiments in Studies of Structural Changes in LNT Materials," Eighth DOE Crosscut Workshop on Lean Emissions Reduction Simulation, University of Michigan–Dearborn, Dearborn, Michigan, May 17–19, 2005.

References

1. W. Deng, M. W. Toepke, and B. H. Shanks, *Adv. Func. Mater.* **13**, 61 (2003).
2. B. C. Gates, *Chem. Rev.* **95**, 511 (1995).
3. C. K. Narula, S. R. Nakouzi, R. Wu, C. T. Goralski, and L. F. Allard, *AIChE Journal* **47**, 744 (2001).
4. M. A. Andrews, S. W. Kirtley, and H. D. Kaesz, *Inorg. Synth.* **17**, 16 (1977).
5. A. S. Fung, P. A. Tooley, M. J. Kelley, D. C. Koningsberger, and B. C. Gates, *J. Phys. Chem.* **95**, 225 (1991).